Toward a self-generating magnetic dynamo: The role of turbulence

Nicholas L. Peffley, A. B. Cawthorne, and Daniel P. Lathrop*

Department of Physics, University of Maryland, College Park, Maryland 20742

(Received 6 July 1999)

Turbulent flow of liquid sodium is driven toward the transition to self-generating magnetic fields. The approach toward the transition is monitored with decay measurements of pulsed magnetic fields. These measurements show significant fluctuations due to the underlying turbulent fluid flow field. This paper presents experimental characterizations of the fluctuations in the decay rates and induced magnetic fields. These fluctuations imply that the transition to self-generation, which should occur at larger magnetic Reynolds number, will exhibit intermittent bursts of magnetic fields.

PACS number(s): 47.27.−i, 47.65.+a, 05.45.−a, 91.25.Cw

I. INTRODUCTION

The generation of magnetic fields from flowing liquid metals is being pursued by a number of scientific research groups in Europe and North America. Nuclear engineering has facilitated the safe use of liquid sodium, which has contributed to this new generation of experiments. With the highest electrical conductivity of any liquid, sodium retains and distorts magnetic fields maximally before they diffuse away. The stretching of field lines by the flow may lead to amplification, but only if it overcomes the resistive damping. This competition between stretching and dissipation is quantified by the magnetic Reynolds number $Re_m = UL/\eta$ [in which U is a characteristic velocity, L a characteristic length scale, and $\eta = 1/(\sigma\mu_0)$ is the magnetic diffusivity composed of the electrical conductivity σ and the magnetic permeability μ_0].

The essential ingredients of a self-generating dynamo are twofold: the proper velocity field and a sufficiently large Re_m for that velocity field. Hints of a good (in the sense of self-generating at a low Re_m) velocity field can be gained from the literature discussing the kinematic dynamo problem [1,2,16]. Kinematic dynamo research has explored in detail different types of laminar (analytic) velocity fields and their efficacy in magnetic field generation [3,4]. Qualitative ideas have emerged from these studies indicating that velocity fields with helicity are important. Velocity fields possessing strong hyperbolic points, allowing maximal stretching, may also be important. Our experiments are motivated by the kinematic dynamo results of Dudley and James [4], who studied a variety of velocity patterns in a spherical volume and their ability to self-generate.

Sharp differences exist between the picture of transition to self-generation motivated by kinematic dynamo studies (on laminar flow fields) and that from experiments that always show turbulence. An important parameter that illustrates this difference is the magnetic Prandtl number $Pr_m = \nu/\eta$, where ν is the kinematic viscosity. The (hydrodynamic) Reynolds number $Re = UL/\nu$ is simply related to the magnetic Reynolds number by $Re = Re_m/Pr_m$. As Pr_m is quite small for all liquid metals ($Pr_m = 8.3 \times 10^{-6}$ for sodium at 120 °C), the

Reynolds number will be quite large for all flows attempting to self-generate (where $Re_m \gg 1$ yields $Re \gg 10^5$)—implying turbulent flow. These turbulent flows will cause the transition to self-generation to be intermittent, showing both growth and decay of magnetic fields irregularly in space and time. This intermittency is not something addressed by kinematic dynamo studies. The analysis in this paper focuses on three main points: we quantify the approach to self-generation with increasing Re_m, characterize the turbulence of induced magnetic fields, and discuss the significant effects turbulence will have on the nature of the transition to self-generation.

II. APPARATUS

Our apparatus (Fig. 1) consists of a 31.2 ± 0.5 cm hollow sphere forging of 304 nonmagnetic stainless steel 0.95 cm thick. The flow is driven by two (usually counter-rotating) mixing propellers [5] on 2.54 cm diameter shafts entering from either pole. Each shaft is belt driven by 7.5 kW electric motors controlled by variable frequency drives which control the rotation rate and report the electrical power delivered to
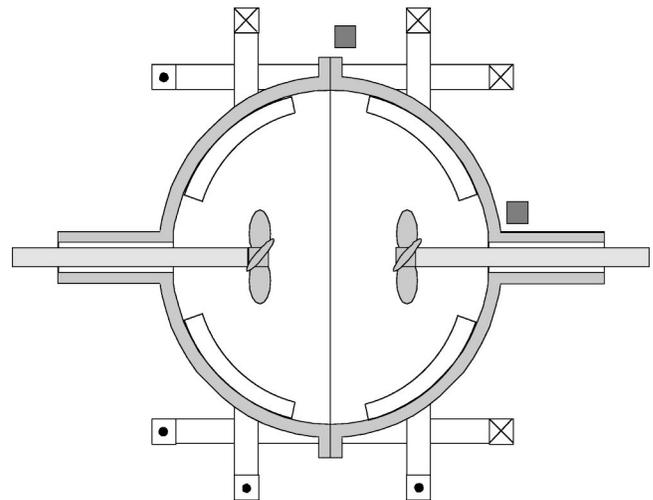

FIG. 1. A cross section of the apparatus shows the location of the propellers that apply forcing, the magnetic coils that supply external applied magnetic fields, and the baffles that enhance poloidal flow.

*Electronic address: dpl@complex.umd.edu

PRE <u>61</u> 5287

TABLE I. Important dimensional parameters for the experiment.

Symbol	Description	Value
b	Propeller radius	6.35 cm
a	Sphere radius	15.24 cm
Ω	Typical angular rotation rate	314.15 rad/s
η	Magnetic diffusivity at 120 °C	830 cm^2/s
ν	Kinematic viscosity at 120 °C	7.39×10^{-3} cm^2/s

the motors. Optical pickups independently monitor the rotation rate of each shaft.

We define the magnetic Reynolds number for our apparatus using the maximum velocity in the system and the radius of the sphere:

$$\mathrm{Re}_m = \frac{UL}{\eta} = \frac{\Omega b a}{\eta}, \qquad (1)$$

where $U = \Omega b$ is the tip speed of the propeller of radius b, and a is the radius of the sphere. Table I shows the important dimensional parameters for the apparatus. By rotating our propellers from 10 to 120 Hz, we can achieve magnetic Reynolds numbers from 7 to 80. The maximum rotation rate is set by the available power from the motors as discussed in Sec. IV. We maintain the sodium near a constant temperature of 120 °C. External heaters supply up to 2.8 kW in order to keep the sodium above the melting point of 97.6 °C. The temperature of the sodium is monitored by a thermocouple placed 1 cm into the liquid. The propellors inject mechanical power into the liquid sodium, and this mechanical power is converted into heat through the action of viscosity. Hexane flowing though 16 m of 1.27 cm diameter copper tubing in thermal contact with the sphere provides up to 8 kW of cooling. Both the heating and cooling are controlled in order to maintain the sodium at 120 ± 5 °C. At the highest rotation rates, we inject approximately 15 kW of mechanical power, and we are unable to provide enough cooling. Thus, only brief experiments at these rotation rates are possible. An external magnetic field is produced by two Helmholtz coil pairs, one pair mounted coaxially with the shafts, and one pair mounted at right angles to the shaft. For the decay measurements, current is pulsed to the coils for 1 to 10 s and rapidly turned off (~ 1 ms) by insulated gate bipolar transistor (IGBT) semiconductor switches. The magnetic fields are monitored by Hall probes maintained at constant temperature and placed close to the surface of the sphere. Nitrogen is used to purge the experiment prior to each run. The sodium is transferred to the experiment by using nitrogen pressure applied to the storage tank. After an experimental run the sodium is transferred back to storage using nitrogen, and the experimental apparatus is cleaned. Elastomeric seals (Viton) are used to seal the shafts and are replaced after each run. Proper safety garments, overhead ventilation, a large thermal mass table, fire fighting equipment on hand, and training ensure safety.

We should note that at higher rotation rates (>60 Hz) vigorous cavitation is heard. A 5 psi overpressure is used to partially suppress the cavitation. Larger overpressures could be used but hasten leaking at the shaft seals. In order to accommodate volume changes in the sodium due to temperature changes or cavitation, the sphere was left connected to the storage tank via a 0.95 cm diameter heated tube.

Dudley and James [4] noted that the ratio of poloidal flow (flow in the direction of the pole) to toroidal flow (azimuthal or rotating flow) is important for dynamo action to occur in the simple velocity fields they studied. Thin stainless steel baffles that run from pole to equator in each hemisphere (see Fig. 1) and extend 5% of the sphere diameter into the flow increase the poloidal component of the velocity field while decreasing the toroidal component. With no baffles in place, we measure no appreciable shift in decay rates. The 5% baffles caused significant changes in the decay rates, while wider (10%) baffles only slightly modified these results. These baffles change the ratio of poloidal to toroidal flow and also break the axisymmetry in the geometry of the system. We have not observed appreciable modification to the magnetic field spectra discussed in Sec. VI from these baffles.

III. EQUATIONS OF MOTION

The governing equations for this flow are well known although not analytically solvable at our parameter values. First is the Navier-Stokes equations for the fluid flow with the added body force, the Lorentz force, which comes into play when the magnetic forces have a back reaction on the velocity field:

$$\frac{\partial \vec{v}}{\partial t} + (\vec{v} \cdot \vec{\nabla})\vec{v} = -\frac{1}{\rho}\vec{\nabla}P + \nu\nabla^2\vec{v} + \frac{1}{\rho}\vec{J} \times \vec{B}. \qquad (2)$$

The Navier-Stokes equation is coupled to the incompressibility condition:

$$\vec{\nabla} \cdot \vec{v} = 0. \qquad (3)$$

No-slip boundary conditions apply at the sphere surface and on the surface of the propellers. The irregular geometry makes handling these boundary conditions (theoretically or numerically) difficult. Ampère's law ($\vec{\nabla} \times \vec{B} = \mu_0\vec{J}$) allows the Navier-Stokes equation to be written in terms of the velocity and magnetic fields only. The magnetic field is governed by the induction equation, which is simply derived from Maxwell's equations and Ohm's law for a moving conductor:

$$\frac{\partial \vec{B}}{\partial t} = \vec{\nabla} \times \vec{v} \times \vec{B} + \eta\nabla^2\vec{B}. \qquad (4)$$

In addition to the Reynolds number and the magnetic Reynolds number already discussed, another dimensionless parameter important in these equations is the Lundquist number. The Lundquist number characterizes the magnetic Reynolds number for Alfvén waves $S = v_a b/\eta$, where $v_a = B/\sqrt{\rho\mu_0}$ is the Alfvén velocity in a magnetic field B and b is the radius of the propeller (see Table I). For the 120 G applied pulse fields we use, $S = 0.67$, showing that our system is marginally able to support Alfvén waves. Interesting future experiments may involve larger external applied magnetic fields (and thus larger S), yielding a state with fully developed magnetohydrodynamic (MHD) turbulence.

IV. POWER DISSIPATION

The practical limit on the magnetic Reynolds number achievable in any experiment is set by the mechanical power available. The power scaling in the Kolmogorov limit (viscosity independent) is

$$P = c_f \rho a^2 b^3 \Omega^3 = c_f \frac{\rho \eta^3}{a} \mathrm{Re}_m^3, \qquad (5)$$

where we define c_f as the (skin friction) coefficient for the scaling. Our power dissipation measurements (Fig. 2) are supplied by the variable frequency drives that power our electric motors. These measurements have confounding errors associated with drag and inefficiencies of the motors, belt drives, bearings, and seals of the apparatus. Nevertheless, at larger rotation rates our results rapidly approach the Kolmogorov scaling and yield an estimate of the friction coefficient (Fig. 3). These measurements were not found to follow a Prandtl–von Karman scaling involving logarithmic corrections [6,7]. Logarithmic corrections usually observed in smooth wall power (drag) scaling are absent for propeller driven flows dominated by pressure drop terms for the propeller.

V. EIGENVALUE MEASUREMENTS

In order to measure the distance from self-generation, we examine the decay of externally applied fields [8,9]. Interpreting these measurements involves viewing the induction equation [Eq. (4)] as an eigenvalue problem for $\vec{B}$, given a time-independent velocity field $\vec{v}$,

$$\vec{B} = \sum_{i=0}^{\infty} \exp(\lambda_i t) B_i(\vec{r}),$$

$$\lambda_i \vec{B}_i = \vec{\nabla} \times \vec{v} \times \vec{B}_i + \eta \nabla^2 \vec{B}_i. \qquad (6)$$

Here λ_i are the eigenvalues associated with eigenmodes of the magnetic field $\vec{B}_i$. If $\vec{v}$ is not stationary, but periodic in time, Floquet theory permits similar analysis. If the velocity field is turbulent, no exact solution is possible. A mean-field approximation would involve replacing $\vec{v}$ with the time-averaged velocity field in Eq. (6). Results from the experiments of Gailitis *et al.* partially support this mean-field view [10]. Even without using the mean-field approximation for the role of the velocity field in the induction equation, short-term decay measurements can be viewed as a short-term Lyapunov exponent. Averages of these short-term exponents then yield the Lyapunov exponents for the magnetic field.

We estimate the leading eigenvalue for the magnetic field by a pulse decay technique. A 1 s pulse of magnetic field (about 120 G) is externally applied with Helmholtz coils, then the current to the coils is rapidly (<1 ms) turned off [Fig. 4(a)]. The magnetic field monitored near the sodium decays nearly exponentially [Fig. 4(b)], as expected from the analysis of the induction equation. The slope of this decay is estimated using a least squares procedure at times after shorter decay modes have disappeared ($t > 0.01$ s) and before noise dominates the signal ($t < 0.1$ s). The slope is taken
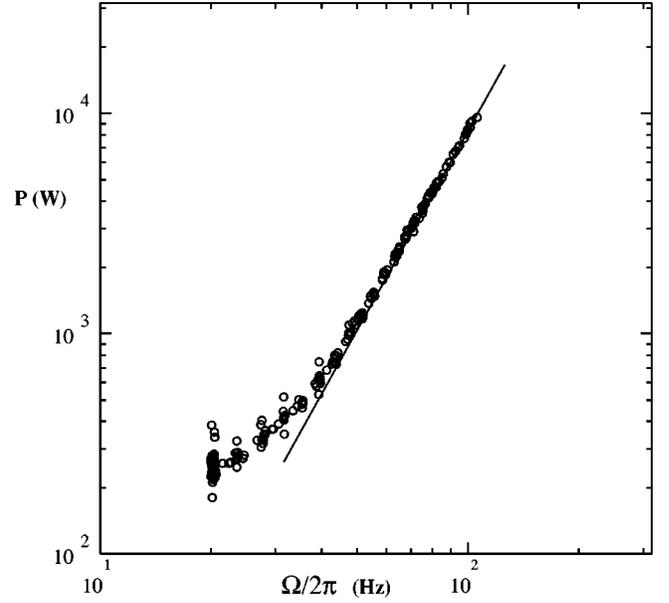

FIG. 2. The mechanical power supplied to the apparatus as a function of the rotation rate. The Kolmogorov scaling of $P \sim \Omega^3$ is shown by a line which agrees with the observations at large rotation rates. The deviation at smaller rotation rates is likely influenced by losses in the seals and motor inefficiencies.

as an estimate of the eigenvalue and faithfully characterizes the short-term decay [Fig. 4(c)].

The eigenvalue for a conducting sphere in the case of zero velocity (the purely resistive case) is found to be $\lambda_r = \pi^2 \eta / r^2$ [1]. For sodium at 120 °C, the magnetic diffusivity is $\eta = 830$ cm^2/s. For our sphere of radius $r = 15.6$ cm, one then obtains $\lambda = -33.6$ s^{-1}, in good agreement with the experimentally obtained value of $\lambda = -34.2$ s^{-1}. This gives a diffusion time scale of about 29 ms for $\mathrm{Re}_m = 0$. These
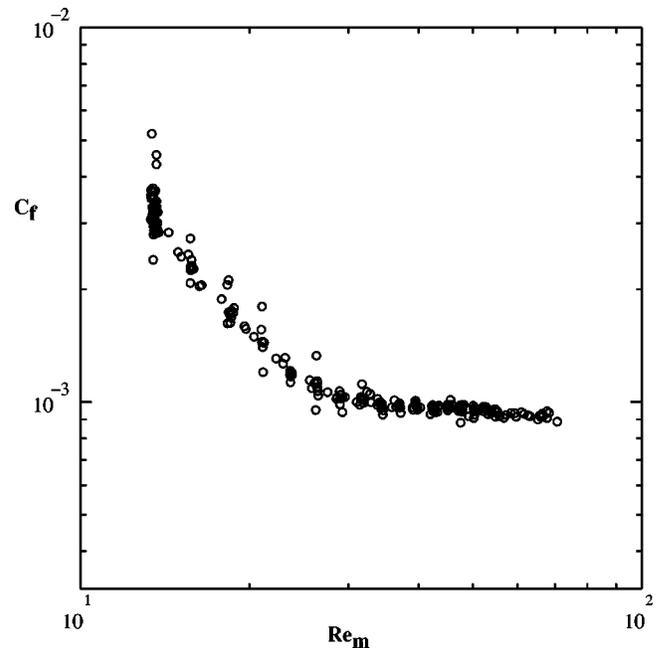

FIG. 3. The skin friction coefficient $c_f = P/\rho a^2 b^3 \Omega^3$ approaching a constant value shows the approach to the Kolmogorov scaling for the power dissipation.
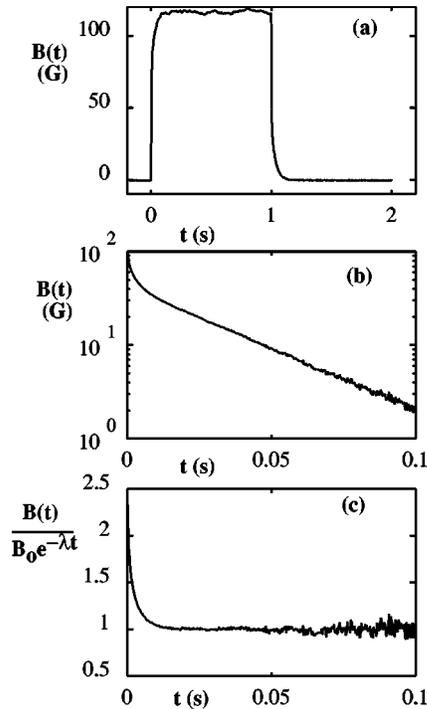
FIG. 4. Externally applied pulses of magnetic field are used to estimate the leading eigenvalue for the magnetic field. A typical pulse (a) at $Re_m = 42$ shows the 1 s pulse, fluctuations on the pedestal, and the decay after the current is cut to the coils. A magnified view (b) plotted semilogarithmically after the external current has been stopped shows the asymptotic exponential decay and slope used for the eigenvalue estimate. (c) shows the same data as in (b) divided by the estimated exponential function.

eigenvalue measurements are sensitive to the temperature of the sodium due to the temperature dependence of the magnetic diffusivity (through the resistivity). Observations of this dependence are shown in Fig. 5. The linear coefficient (observationally 0.22% per °C) is in good agreement with past observations of the resistance temperature coefficient (0.31% per °C) [11].

A trend toward self-generation can be observed in the eigenvalue dependence on magnetic Reynolds number (Fig. 6). For applied magnetic pulses aligned with the shafts, the eigenvalues show a trend toward zero, the threshold to self-generation. This trend indicates that the fields decay more slowly as the magnetic Reynolds number is increased. For applied magnetic fields at right angles to the shafts, the opposite trend is observed. If we consider only the mean velocity field, these two trends stand in contrast to the predictions from Dudley and James [4], where self-generation occurs at $Re_m = 54$ for magnetic fields at right angles to the axis of symmetry. Moreover, for purely axisymmetric velocity fields, only nonaxisymmetric magnetic fields can self-generate (due to Cowling's theorem [12]). Thus, the nonaxisymmetric features of our velocity field must be playing an important role in the trend toward magnetic field generation. Three important sources of nonaxisymmetric velocity components exist: the three-lobed propellers, the four sets of baffles running pole to pole, and turbulent fluctuations. Unfortunately, there is no known method to express an analytical velocity field incorporating these aspects of the velocity field.
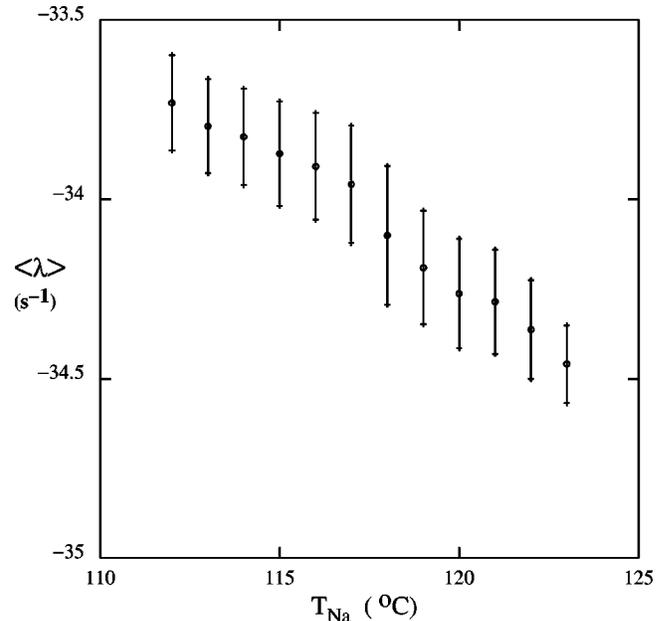

FIG. 5. The eigenvalues are a strong function of the mean temperature of the sodium—here shown for no flow ($Re_m = 0$). This nearly linear dependence comes from the temperature dependence of the resistivity. This dependence necessitates both good temperature control of the experiment and correction of eigenvalue measurements for the remaining drift.
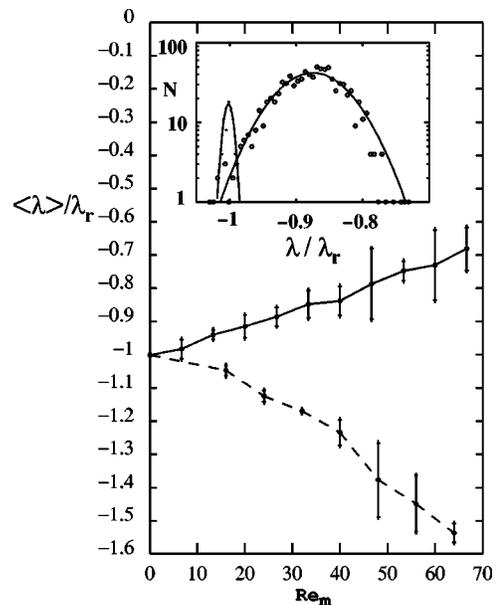

FIG. 6. The mean eigenvalue dependence on magnetic Reynolds number shows a shift toward self-generation for fields aligned with the shafts (solid line) and a shift away from self-generation for fields at right angles to the shafts (dashed line). The error bars indicate shot-to-shot fluctuations in the eigenvalue estimates. These fluctuations are further quantified by the distribution of eigenvalues shown in the inset for 895 observations of the eigenvalue at the same $Re_m = 42$. All the eigenvalues in this figure are normalized to yield -1 in conditions of no flow. The distribution for no flow ($Re_m = 0$) is shown in the inset by the narrow Gaussian around -1. Presumably, the self-generating state is achieved if we cross the $\lambda = 0$ line.
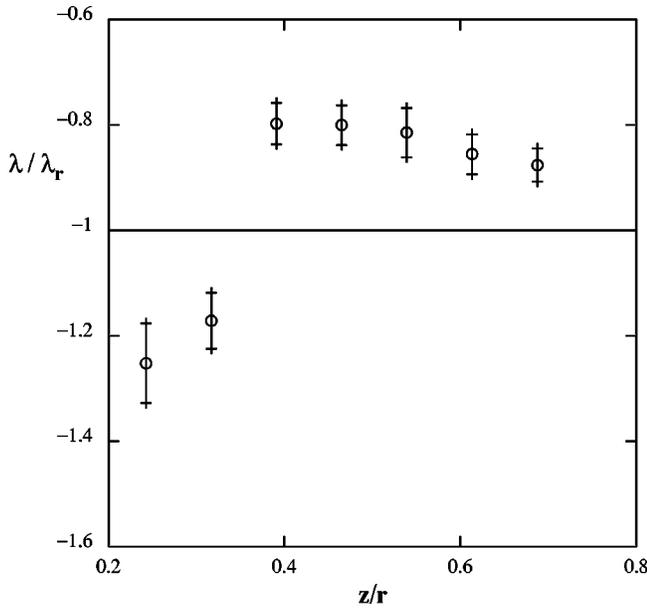
FIG. 7. The eigenvalue shifts show a strong dependence on the geometry of the flow. Here we have varied the axial position of both propellers relative to their abutting at the equatorial plane ($z/r=0$).

Significant fluctuations occur between different pulse decay eigenvalue estimates while the experimental parameters (temperature, rotation rates) are kept fixed. These fluctuations are quantified both by the error bars in Fig. 6 and by the probability distribution shown in the Fig. 6 inset. The distribution appears to be near-Gaussian and has a width comparable to the observed shifts of the eigenvalue. The effects of turbulent velocities can be seen in the width of the distribution of decay rates at nonzero Re_m. Due to the small Pr_m, the system will have a large Re for moderate Re_m, and thus one would expect turbulent velocity profiles. The broad width of the decay rates for a given nonzero Re_m is a good indication that the turbulence in the velocity field is playing an important role in the decay rate of the pumped sodium. The broad distribution of the decay rates allows a prediction of the form of the transition to self-generation. As the mean shift approaches zero (near the crossover from damped magnetic fields to growing magnetic fields), the events associated with the positive tail of the distribution will cause growth of fields local in time. This local growth will lead to an intermittent state near transition characterized by large excursions between growing and damped fields. Once the fields become large enough to cause back reaction through Lorentz forces, this picture may change.

The eigenvalue shifts are significantly affected by changes in the flow geometry. Figure 7 shows observations of the changes in the eigenvalues as the shafts are translated axially. When the propellers are quite close together, the damping of the magnetic field is enhanced ($\lambda/\lambda_r<-1$). The sudden change from $\lambda/\lambda_r<-1$ to $\lambda/\lambda_r>-1$ at $z/r=0.35$ appears to be a discontinuity. Experiments performed around this geometrical configuration have shown transients of $\lambda/\lambda_r>-1$ give way to faster-than-resistive decay after a few minutes. As might be expected for such a strongly turbulent state, no hysteresis was observed.

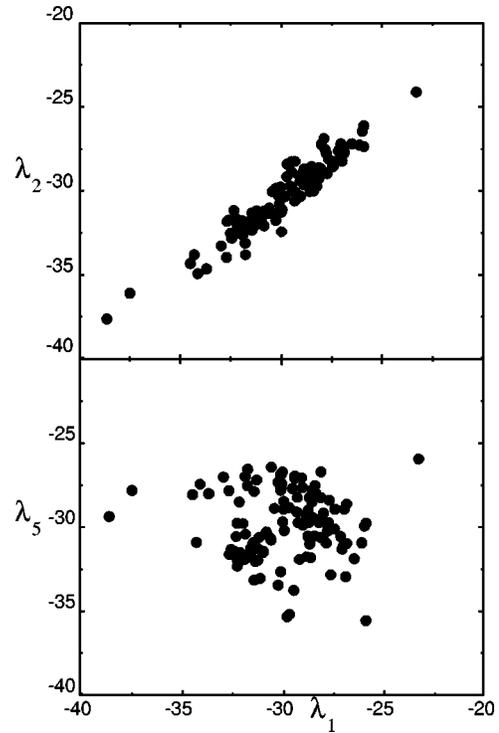Data on spatial correlations were obtained using a circular

FIG. 8. A scatter plot of the eigenvalues simultaneously measured at two different Hall probes. λ_1 and λ_2 represent decay rates of adjacent Hall probes while λ_1 and λ_5 represent decay rates of hall probes separated azimuthally by 96°. The strong dependence in the λ_1-λ_2 plot and the weak dependence in the λ_1-λ_5 plot illustrate the decay in correlation as separated probes are compared. These data are taken at $\mathrm{Re}_m=42$.

array of Hall probes. This array is 15 cm in diameter and contains 15 Hall probes equally spaced azimuthally. The array is coaxial with the shafts and in contact with the sphere. Eigenvalue estimates are made at all 15 Hall probe locations, and simultaneous estimates are compared. Scatter plots of the eigenvalues measured at different probes simultaneously are shown in Fig. 8. Adjacent probes show a strong correlation which drops off rapidly with angular distance. This decorrelation is quantified in Fig. 9. By a 90° angular dis-
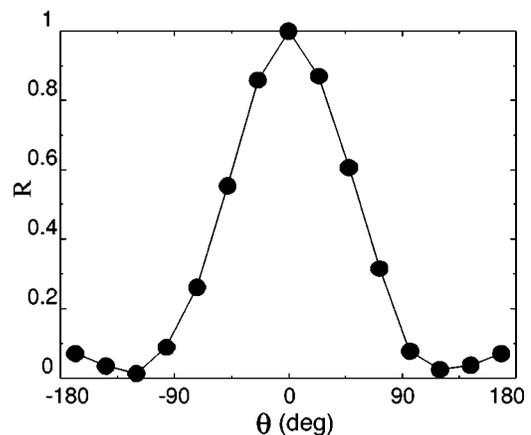

FIG. 9. The coefficient of regression ($R=1$ gives perfect linear dependence) from linear regressions of instantaneous eigenvalues from Hall probes separated by an azimuthal angle Θ. These data are taken at $\mathrm{Re}_m=42$.
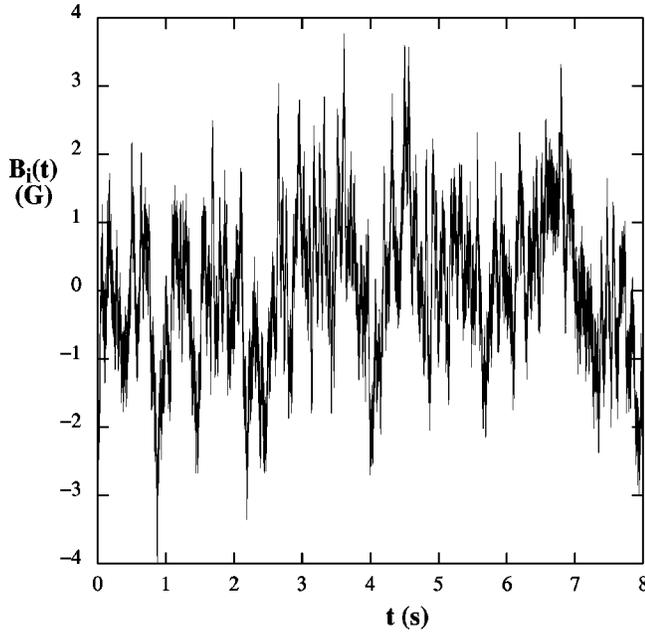
FIG. 10. Typical fluctuations in the induced field as on the pedestal shown in Fig. 4(a). The mean applied field (120 G) and the induced field (-17 G) at $Re_m = 33$ have been subtracted, leaving only mean zero fluctuations. These fluctuations are broadband and have their root in the underlying fluid turbulence observed at $Re_m = 33$. Instrumental noise has an amplitude of about 0.1 G.

tance the eigenvalues have lost all correlation. A slight increase in correlation is seen at 180°. These data indicate that the eigenvalue fluctuations are a local phenomenon and are likely closely coupled to the turbulent state.

VI. MAGNETIC FIELD FLUCTUATIONS

During a magnetic field pulse, the applied external field gives rise to induced currents and induced magnetic fields in the sodium. Typical fluctuations of the induced fields are shown in Fig. 10. The induced fields and their broadband fluctuations depend on the magnetic Reynolds number, generally increasing in size and variation as Re_m is increased (Fig. 11). Three different types of predictions for the spectrum of magnetic field fluctuations can be found in the literature [13–15]. We might categorize them as (1) vorticity analogy, (2) MHD turbulence, and (3) weak field predictions.

In the case in which the magnetic energy is small compared to the kinetic energy, an analogy between the vorticity and the magnetic field has been made. This analogy predicts that the Kolmogorov spectra for vorticity should be observed for magnetic field fluctuations $E_\omega \sim E_B \sim k^{1/3}$ [13].

Another prediction comes from the theory of fully developed MHD turbulence. There, the kinetic and magnetic energy spectra are thought to come into equipartition, yielding a state with $E_k \sim E_B \sim k^{-3/2}$ [13].

Finally, the weak field case applies when the magnetic field can be split into $\vec{B} = \vec{B}_0 + \vec{B}_1$ with the large external field $\vec{B}_0$, the induced fluctuations $\vec{B}_1$, and $\vec{B}_0 \gg \vec{B}_1$. We can understand the source of scaling by looking at the induction equation [Eq. (4)] in Fourier space:

$$i\omega \vec{B}_{\omega,k} = i\vec{k} \times \vec{v}_{\omega,k} \times \vec{B}_0 - \eta k^2 \vec{B}_{\omega,k}, \qquad (7)$$
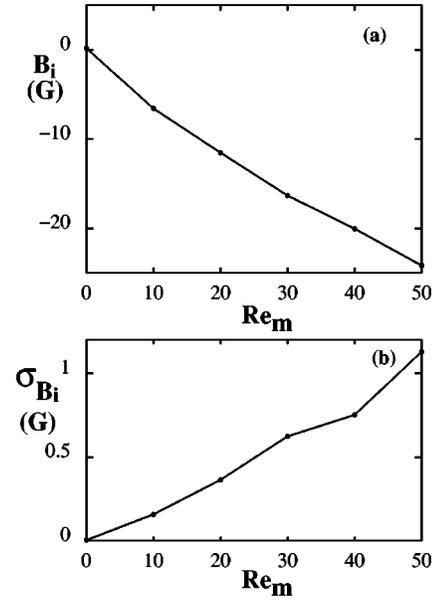

FIG. 11. Statistics of the induced field as a function of Re_m. The mean induced field (a) aligned with shaft axis is opposite the external applied field. Fluctuations increase (b) with increases in magnetic Reynolds number.

where $\vec{B}_{\omega,k}$ is the Fourier transformed induced magnetic field, $\vec{v}_{\omega,k}$ is the Fourier transformed velocity field, and $\vec{B}_0 = B_0 \hat{z}$ is the structureless applied magnetic field.

There are two interesting limits to the behavior when the induced field is still too small to cause any back reaction on the velocity field [14,15]. In one case, the first and second terms of Eq. (7) balance (stirring dominates). Alternatively, the second and third terms will balance if diffusion dominates. The crossover between these two cases occurs when $v/\eta k$ (a type of magnetic Reynolds number) is unity. On dimensional grounds, we can estimate the form of the induced magnetic field spectra which, in the first case, yields

$$\frac{B_{\omega,k}}{B_0} \sim \frac{k v_{\omega,k}}{\omega}. \qquad (8)$$

A dispersion relation (information about ω/k) must be used to further study this case. If a large mean velocity is rapidly sweeping structures past, we might invoke Taylor's hypothesis and obtain from Eq. (8) that the magnetic energy spectra will resemble the kinetic energy spectra $E_B \sim E_k \sim k^{-5/3}$.

In the diffusive case, comparing the second and third terms of Eq. (7), we obtain

$$\frac{B_{\omega,k}}{B_0} \sim \frac{v_{\omega,k}}{\eta k}. \qquad (9)$$

This case is straightforward and yields an estimate of $E_B \sim E_k/k^2 \sim k^{-11/3}$.

Experimental power spectra of the induced fields show a variety of characteristic features. An average of 19 power spectra measured at $Re_m = 33$ is shown in Fig. 12. These spectra usually show small spectral peaks at the rotation rate and three times the rotation rate. These peaks are likely due to fluid motions driven by the (three-lobed) propellers. The peaks showing the influence of the propellers support one
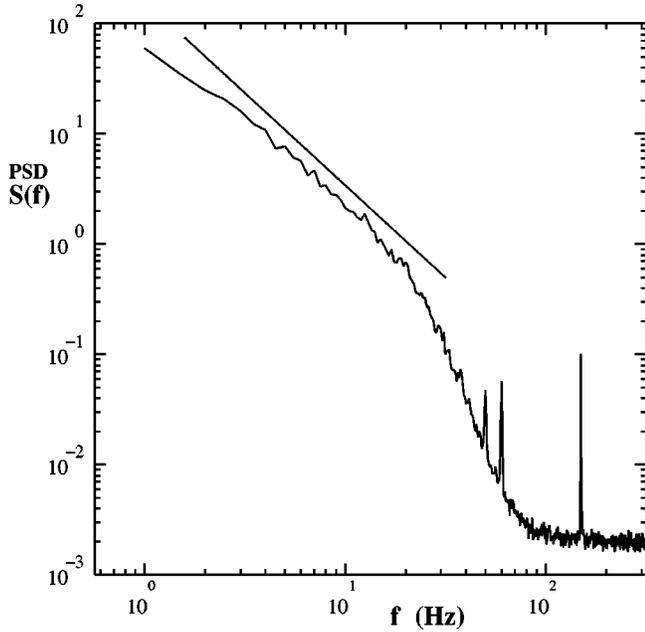
FIG. 12. The power spectral density of induced field fluctuations shows broadband turbulent features including a power law decay at low frequency. An offset line is shown with the best fit exponent $S(f) \sim f^{-1.68 \pm 0.03}$. This is consistent with the scaling indicated by Eq. (8). Also prominent are peaks at $\Omega/2\pi = 50$ Hz, power line interference at $f = 60$ Hz, and one peak at $3\Omega/2\pi = 150$ Hz. The magnetic Reynolds number for this flow is 33.
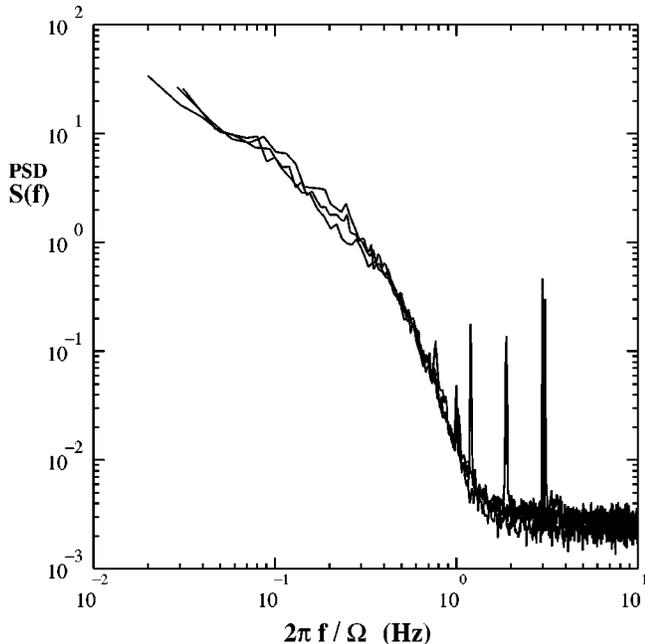

FIG. 13. Power spectra from three magnetic Reynolds numbers (22, 33, and 42) collapse if scaled by the rotation rates. Only the power line frequency changes greatly between the three.
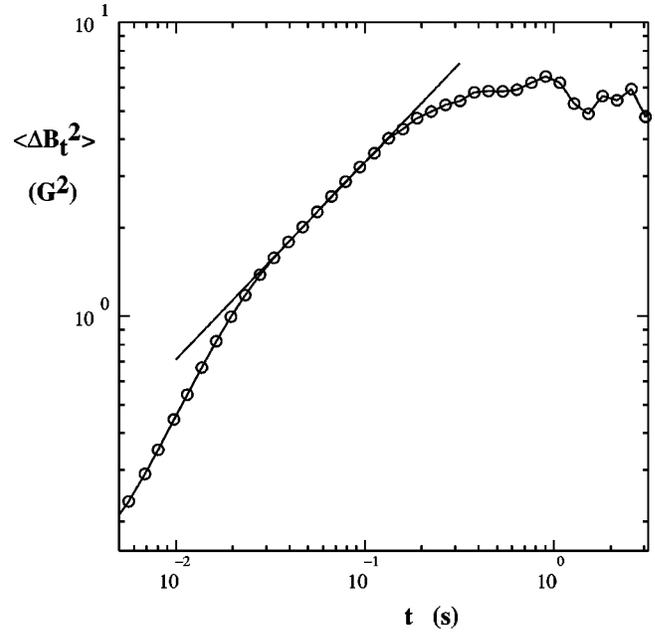

FIG. 14. Comparable information to the power spectra can be obtained from the second order structure function $\langle (B(t'+t) - B(t')^2 \rangle$, here shown for $\mathrm{Re}_m = 33$. The straight line shows a scaling with slope 0.67 ± 0.02 consistent with Kolmogorov scaling for three-dimensional turbulent velocity fluctuations.

source of nonaxisymmetry suggested by the eigenvalue results. Also evident is one peak due to 60 Hz pickup from power lines. At low frequency, the spectra show about a decade of a $f^{-1.69}$ power law scaling. Using Taylor's hypothesis, this scaling can be interpreted as confirmation of the $k^{-5/3}$ spectra predicted by dimensional analysis from the induction equation. This observed scaling supports the hypothesis that the external fields are too small to have influenced the flow field significantly.

Detection of high frequency magnetic fields will be hampered by the shielding caused by the 1 cm thick stainless steel sphere surrounding the sodium. The skin depths for 304 stainless steel at 1 , 10, 100, and 1000 Hz are approximately 42, 13, 4, and 1 cm, respectively. We observe a crossover between Kolmogorov scaling and a more rapid falloff in the magnetic field spectrum at approximately 20 Hz. The subsequent drop in power (approximately $f^{-4.5}$) is steeper than predicted in the $f^{-11/3}$ dissipative range scaling for the induction equation and at a lower frequency than the damping one would expect due to shielding from the conducting boundary at these frequencies. Magnetic field shielding will become important when the skin depth is comparable to the wavelength, which for this system occurs at $f \sim 1000$ Hz. Although the damping of the signals includes losses due to shielding, the crossover and the subsequent falloff are most likely due to the Hall probe distance (2 cm) from the surface of the sodium. Field structures smaller than this probe distance will be exponentially damped at the probe.

In order to account for the specific observed frequency crossover, a velocity estimate for 2 cm structures is needed. As these fine scale structures are within the hydrodynamic boundary layer, a velocity scale for the boundary is needed; we use the shear velocity $u^* = \sqrt{\tau_w/\rho}$ which characterizes logarithmic boundary layers [16] (where τ_w is the wall shear stress). At $\mathrm{Re}_m = 33$, the shear velocity (calculated from knowledge of the power dissipation) yields $u^* = 69$ cm/s. This velocity taken with the probe separation from the sphere then gives a crossover frequency estimate of 34 Hz, which is consistent with the observed crossover.

As the magnetic Reynolds number increases, no signifi-

cant changes in the power spectra are observed. Three spectra from magnetic Reynolds numbers $Re_m = 22, 33,$ and 42 are shown in Fig. 13. The spectra have been scaled by the rotation rates of the propeller and collapse reasonably well.

A further test of the observed Kolmogorov spectra is shown in the second order structure function (Fig. 14). The scaling here also supports the existence of Kolmogorov spectral behavior for the induced fields.

VII. CONCLUSIONS

Experimental observations have quantified the approach to magnetic field self-generation in flows of liquid sodium. The turbulence of this flow leaves signatures both in eigenvalue fluctuations and in fluctuations in the induced magnetic field. These observations in turn yield predictions that the transition to self-generation will be intermittent, yielding local sporadic growth of magnetic fields close to transition.

ACKNOWLEDGMENTS

[1] H.K. Moffatt, *Magnetic Field Generation in Electrically Conducting Fluids* (Cambridge University Press, Cambridge, 1978).

[2] P.H. Roberts, *An Introduction to Magnetohydrodynamics* (Elsevier, New York, 1967).

[3] E. Bullard and H. Gellman, Philos. Trans. R. Soc. London, Ser. A **247**, 27 (1954).

[4] M.L. Dudley and R.W. James, Proc. R. Soc. London, Ser. A **425**, 407 (1989).

[5] 5×5 left-handed mixing propeller, McMaster-Carr Supply Company, part number 8004K161.

[6] H. Schlichting, *Boundary-Layer Theory*, 7th ed. (McGraw-Hill, New York, 1979), pp. 598 and 639.

[7] D.P. Lathrop, J. Fineberg, and H.L. Swinney, Phys. Rev. Lett. **68**, 1515 (1992); Phys. Rev. A **46**, 6390 (1992).

[8] N.L. Peffley, A.G. Goumilevski, A.B. Cawthorne, and D.P. Lathrop (unpublished).

[9] A. B. Cawthorne, N. L. Peffley and D. P. Lathrop, Geophys. J. Int. (to be published).

[10] A.K. Gailitis, B.G. Karasev, I.R. Kirillov, O.A. Lielausis, S.M. Luzhanskii, and A.P. Ogorodnikov, Magnetohydrodynamics **23**, 349 (1987).

[11] *Liquid-Metals Handbook: Sodium NaK Supplement* (Atomic Energy Commission, Washington, D.C., 1955).

[12] M. Ghil and S. Childress, *Atmospheric Dynamics, Dynamo Theory, and Climate Dynamics*, Vol. 60 of Topics in Geophysical Fluid Dynamics, edited by Fritz John, J.E. Marsden, and Lawrence Sirovich (Springer-Verlag, Berlin, 1987).

[13] D. Biskamp, *Nonlinear Magnetohydrodynamics* (Cambridge University Press, Cambridge, 1993).

[14] P. De Michelis, G. Consolini, and A. Meloni, Phys. Rev. Lett. **81**, 5023 (1998).

[15] P. Odier, J.-F. Pinton, and S. Fauve, Phys. Rev. E **58**, 7397 (1998).

[16] M.R.E. Proctor and A.D. Gilbert, *Lectures on Solar and Planetary Dynamos*, Publications of the Newton Institute (Cambridge University Press, Cambridge, 1994).